Thermocline Forced by Varying Ekman Pumping. Part II: Annual and Decadal Ekman Pumping

ZHENGYU LIU

UCAR Visiting Scientist Program, Department of Atmospheric and Oceanic Sciences, Princeton University, Princeton, New Jersey

(Manuscript received 16 January 1992, in final form 14 August 1992)

ABSTRACT

Thermocline variability forced by zonally uniform Ekman pumping with annual to decadal periods is investigated. Both analytical and numerical solutions are obtained by the method of characteristics. As found in Part I, there is little thermocline variability in the ventilated zone or pool zone. In contrast, strong variability may exist in the shadow zone.

For annual forcings, nonlinearity is negligible. However, the linear solution is influenced substantially by the basic-state thermocline structure. As a result, local responses dominate for a shallow interface, while remote Rossby waves dominate for a deep interface.

Under a strong decadal forcing, nonlinearity may become important. The time-mean thermocline in the shadow zone is shallower than the steady thermocline under the mean Ekman pumping, particularly in the western part of a shadow zone where the mean deviation may reach the order of ten meters. This shallower mean thermocline is caused by the nonlinear Rossby wave.

1. Introduction

In a previous paper (Liu 1993a, hereafter referred to as LIU), a two-layer planetary geostrophic model is used to investigate the evolution of a ventilated thermocline in response to a sudden change of Ekman pumping. This spinup problem is particularly successful in highlighting the physics behind the evolution. It is found that the dynamics differs dramatically between a shadow zone and a ventilated zone. In a shadow zone, the local Ekman pumping is mainly balanced by the Rossby wave propagation, whereas in a ventilated zone the Ekman pumping is mainly opposed by cold advection from the north. As a result of the different dynamics, thermocline variability also varies substantially between the two zones. After a sudden change in Ekman pumping, the shadow zone exhibits strong thermocline variability, while the ventilated zone has little thermocline variation.

However, some important issues cannot be understood in the spinup case. For example, observations clearly show that the variation amplitude of isopycnal surfaces differs dramatically for different time scales. Therefore, as a further step, several other issues will be addressed in this paper. First, how does a thermocline evolve under an annual or a decadal wind forcing? Most previous works, whether theoretical, numerical, or observational, have concentrated on annual variability. On the other hand, recent interest in climate change also requires understanding of decadal variability. Therefore, the decadal forcing needs particular attention. Physically, on an annual time scale, a midlatitude Rossby wave crosses only a fraction of the width of the basin, while on a decadal time scale, a Rossby wave is able to cross an entire ocean basin. Therefore, decadal variability may have different features from those of annual variability.

Second: what is the effect of the two-dimensional thermocline structure and flow on the propagation of planetary waves? Most previous works have investigated the local response or the linear Rossby wave in the absence of a mean thermocline circulation. However, the wave speed of a baroclinic planetary wave in the midlatitudes is comparable to that of the mean wind-driven flow. In addition, the observed mean thermocline structure varies significantly in space. Thus, we may expect significant influence arising from the mean flow and thermocline. Indeed, preliminary studies on waves in the presence of a zonal baroclinic flow have shown that the Rossby wave propagation could be changed substantially (e.g., Anderson and Killworth 1979; Cheng and Philander 1989). Here, we will further explore the thermocline variability in the presence of a two-dimensional flow and thermocline structure. In particular, as a recent concern, we are interested in the relative importance of the local Ekman pumping and the Rossby waves radiating from the eastern boundary. Classical works claimed the local Ekman pumping to be the main driving mechanism for the variability (e.g., Gill and Niiler 1973; Roden

Corresponding author address: Dr. Zhengyu Liu, Program in Atmospheric and Oceanic Sciences, University of Wisconsin—Madison, Madison, WI 53706.

1976). However, recent studies show that the local Ekman pumping produces a poor phase correlation with the observation, and underestimates the amplitude of the variability badly (e.g., White and Saur 1983; Kessler 1989). Instead, a model incorporating Rossby waves improves the results substantially in the southern part of the subtropical North Pacific. Here, we will explore this problem from a theoretical viewpoint with an emphasis on the role of the thermocline structure.

Finally, how strong is the nonlinearity? The nonlinearity of Rossby waves and the interaction between the barotropic and baroclinic flows[1] have not been studied extensively. On the other hand, observations have shown that isopycnal variation can often reach ±50 m in the midlatitude main thermocline, with equivalent steric sea-level changes of about ±5 cm (White and Tabara 1987; Tabara et al. 1986; White 1983; Talley and White 1987; Roemmich and Wunsch 1984). If we choose a decorrelation space scale of $L = 1000$ km and a reduced gravity of 1 cm s^{-2}, this thermocline variability corresponds to a disturbance geostrophic velocity $(\gamma/f)(\delta h/L) \approx 1$ cm s^{-1}. This velocity is comparable to the wave speed of planetary waves in the midlatitudes. Therefore, the nonlinear evolution of the thermocline may be important. One concern closely relevant to the nonlinearity is the structure of a time-mean thermocline. This has recently been studied by Dewar (1989), who found that under an annual forcing, the time-mean thermocline has a residual circulation that consists of microgyres in the otherwise motionless shadow zone. However, his model is a quasigeostrophic model, in which the only nonlinearity comes from the barotropic–baroclinic interaction. Here, his work will be extended in two directions: the inclusion of nonlinear Rossby waves and the consideration of decadal time scales.

The paper is arranged as follows. In section 2, we will find that under an annual Ekman pumping with a deviation of, say, 50% from the mean as observed by Levitus (1988), linear waves superimposed on a steady ventilated thermocline approximate the fully nonlinear solution excellently. Even for a decadal forcing, linear wave theory still predicts the thermocline variability very well in the eastern part of a shadow zone. A more comprehensive comparison between linear and nonlinear solutions will be presented in section 3. The linear theory also shows that the basic thermocline structure plays an essential role in determining the relative importance of local responses and eastern boundary planetary waves. Because of different thermocline structures for different depths of interfaces, on shallower interfaces, local responses dominate, while for middle and deep interfaces, remove waves dominate.

In section 3, we investigate the fully nonlinear solution. At an annual frequency, it will be seen that the time-mean thermocline is close to the steady thermocline forced by the time-mean forcing. However, with a strong decadal forcing, the time-mean thermocline could be significantly shallower than the corresponding steady thermocline, particularly in the western part of the shadow zone. Some possible physical mechanisms are also explored.

To further explore the dependence of the thermocline variability on the frequency and amplitude, in section 4, a detailed calculation is carried out. The calculation demonstrates that for annual and weak decadal forcings, the solution is essentially linear. At decadal or even lower frequencies, if the perturbation Ekman pumping is stronger than 1/10 or 1/5 of that of the time-mean Ekman pumping, the nonlinearity is no longer negligible. Finally in section 5, we summarize our results.

2. Linear theory

In this section, we study the linear theory. Later, it will be shown that with an annual forcing or a weak decadal forcing, the linear solution approximates the fully nonlinear solution very well. The linear theory here highlights the physics of planetary wave propagation in the presence of a basic ventilated thermocline. One issue we are particularly interested in is the relative importance of the local Ekman pumping and remote eastern boundary waves.

a. The model

The model is the same as in LIU. It is a two-layer planetary geostrophic model with a flat and rigid bottom at $z = -H$. The upper- and lower-layer densities are ρ_1 and ρ_2, respectively; the interface is at depth h. The equation governing the interface can be derived as (Rhines 1986; Dewar 1987; Liu 1993a)

$$h_t + v_B h_y + [u_B + C(h)]h_x = -(1 - h/H)w_e.$$

Here, u_B, v_B, and $C(h)$ are barotropic velocity components and the speed of the nondispersive Rossby wave $C(h) = -\beta\gamma h(H - h)/f^2H$. Here w_e is the Ekman pumping imposed on the surface; $\gamma = g(\rho_2 - \rho_1)/\rho_2$ is the reduced gravity. Other notations are standard.

Superscripting a dimensional quantity by a star, we have the nondimensional quantities:

$$f = \frac{f^*}{f_n}, \quad \beta = \frac{\beta^*}{\beta_0}, \quad t = \frac{t^*}{T_W},$$

$$x = \frac{x^*}{L}, \quad h = \frac{h^*}{H}, \quad w = \frac{w^*}{W}.$$

Here W, f_n, and β_0 represent respectively the typical Ekman pumping velocity, the Coriolis parameter at

[1] In this paper, the barotropic–baroclinic interaction refers to the density advection $\mathbf{v}_B \cdot \nabla h$ term. More precisely, this term is not a nonlinear effect because it is induced by the known barotropic velocity interacting with the unknown baroclinic field. This term is a variable coefficient term. Nevertheless, since this term can produce a time-mean thermocline different from the steady thermocline with the time-mean forcing, we will call this term a nonlinear effect.

the northern boundary of the subtropical gyre, and the mean β value in a subtropical gyre; $T_W = H/W$ is the time for a particle to move to the bottom of the thermocline with the Ekman pumping vertical velocity; and $L = (\beta_0 \gamma H/f_n^2) \times T_W$ is the zonal spatial scale for a Rossby wave to travel in the time T_W. The above equation for the interface has the nondimensional form

$$h_t + v_B h_f + (u_B + C)h_x = -(1 - h)w_e, \quad (2.1a)$$

where $C(h) = -h(1 - h)/f^2$. With the Sverdrup relation, one can show that the barotropic velocity $(u_B, v_B) = [-(f^2 \int_0^x w_e dx)_f/f, fw_e]$. Here, we have assumed a vanishing barotropic transport into the eastern boundary. In addition, we have used $f = f_0 + \beta y$ to replace the y coordinate and the nondimensional $\beta = 1$ is chosen. With the aid of continuity equation $\nabla \cdot \mathbf{v}_B = w_e$, (2.1a) can be rewritten as the conservation form

$$h_t + \nabla \cdot (\mathbf{v}_B h) + C(h)h_x = -w_e. \quad (2.1b)$$

For simplicity, we choose our Ekman pumping independent of longitude. Furthermore, the periodic Ekman pumping is assumed to be of the form

$$w_e(f, t) = w_0(f) + aw_1(f, t) \quad \text{with} \quad w_1 = w_0(f)g(t). \quad (2.2a)$$

In the remainder of the paper, we will choose $g(t) = \sin\omega t$. Therefore, a represents the strength of the perturbation forcing. The total Ekman pumping $w_e = w_0(f)(1 + a \sin\omega t)$ varies only in its amplitude but not its position. In reality, the wind field may also migrate north–south substantially, as in the case of annual wind. This effect is not included in (2.2a). Here ω is the nondimensional frequency of the forcing. For a mean thermocline depth $H = 600$ m and a mean Ekman pumping velocity of $W \sim 10^{-4}$ cm s^{-1}, the dimensional time scale $T_w = H/W$ is about 20 years. This gives the dimensionless frequencies: *annual* $\omega \sim 100$ and *decadal* $\omega \sim 10$. In physical terms, at an annual frequency, it takes a planetary wave several periods to cross the ocean basin, while at a decadal frequency it takes a planetary wave less than or about one period to reach the western boundary. In addition, w_0 can be seen to be the time-mean Ekman pumping

$$w_0(f) = \langle w_e(f, t) \rangle \sim O(1), \quad (2.2b)$$

where $\langle \quad \rangle = (\omega/2\pi) \int_0^{2\pi/\omega} dt$.

b. The linear solution

With weak perturbation $a \ll 1$, h can be expanded as

$$h = h_0 + ah_1 + a^2 h_2 + \cdots. \quad (2.3)$$

If the barotropic velocity is decomposed into the time-mean component $\mathbf{v}_{B0}$ and the perturbation component $\mathbf{v}_{B1}$, the Ekman pumping (2.2a) and continuity equation require that

$$\mathbf{v}_B = \mathbf{v}_{B0} + a\mathbf{v}_{B1}; \quad \nabla \cdot \mathbf{v}_{B0} = -w_0, \quad \nabla \cdot \mathbf{v}_{B1} = -w_1. \quad (2.4)$$

1) THE BASIC STATE

Substituting (2.2a), (2.3), and (2.4) into (2.1), at the leading order, we obtain the basic-state equation:

$$\nabla \cdot (\mathbf{v}_{B0} h_0) + C(h_0)h_{0x} = -w_0. \quad (2.5)$$

This gives the steady LPS (Luyten, Pedlosky, and Stommel) thermocline in our two-layer model (Luyten et al. 1983). The thermocline structure can be solved following their method, but, for later convenience, we solve it by the method of characteristics. Choosing s as the variable along a characteristic, the characteristic equations for (2.5a) can be written as

$$\frac{df}{ds} = v_{B0} = fw_0(f),$$

$$\frac{dh}{ds} = -(1 - h_0)w_0(f),$$

$$\frac{dx}{ds} = u_{B0} + C = -[f^2 w_0(f)x]_f/f - h_0(1 - h_0)/f^2.$$

This set of equations can be solved as

$$s = \int_{f_i}^{f} d\lambda/\lambda w_0(\lambda) \quad \text{or} \quad f = \hat{f}(s, f_i), \quad (2.6a)$$

$$f/(1 - h_0) = f_i/(1 - h_i), \quad (2.6b)$$

$$2f^2 w_0(f)x = 2f_i^2 w_0(f_i)x_i + h_0^2 - h_i^2. \quad (2.6c)$$

Here, (2.6b) is the recovery of the conservation of potential vorticity of the basic state along a characteristic line, which is derived by the division of the f and h characteristic equations.

To solve the basic state from (2.6), for simplicity, we will adopt a zonal outcrop line at $f = f_0$, a meridional eastern boundary at $x = 0$, and a flat interface at the eastern boundary $h_e(f) = H_s$. The solution over a subtropical gyre generally has a shadow zone adjacent to the eastern boundary, within which all characteristics start from the eastern boundary. The initial conditions for characteristics, subscribed by i, are then $x_i = 0$, $h_i = H_s$. Equation (2.6c) immediately yields the solution

$$h_0^2 = H_s^2 + 2f^2 w_0(f)x \quad \text{for} \quad x > x_{b0}(f). \quad (2.7a)$$

Here x_{b0} is the shadow zone boundary of the basic thermocline and is formed by the characteristics initiating from the corner $x_i = 0, f_i = f_0$.

To the west of the shadow zone, two solutions are possible depending on whether H_s vanishes or not. If $H_s = 0$, there will be a ventilated zone. For $H_s > 0$, there will be no outcrop line within the subtropical gyre, so there is no ventilated zone. Pedlosky and Young (1983) proposed a pool (Rhines and Young 1982) west of the shadow zone. One common feature of the pool zone (as defined by Pedlosky and Young) and the ventilated zone is that their characteristics do not trace back to the eastern boundary. Instead, the characteristics start from the north. More specifically,

for the outcropping case, the northern boundary is simply the outcrop line f_0, where $h = 0 = H_s$, corresponding to a ventilated zone. For the case without outcropping, following Pedlosky and Young (1983), the northern boundary is the gyre boundary $f_n = 1$, where $h = H_s$, corresponding to a pool zone. Hence, the initial condition for f is $f_i = f_0$ for the ventilated zone and $f_i = 1$ for the pool zone. For both cases, the h initial condition is $h_i = H_s$. The solution is derived from (2.6b) directly as

$$h_0 = 1 - (1 - H_s)f/f_0 \quad \text{for} \quad x < x_{b0}(f). \tag{2.7b}$$

Equations (2.7a,b) give solutions for the steady thermocline for any $h_e(f) = H_s = \text{const}$. Finally, we discuss the characteristics. This turns out to be necessary in deriving explicit solutions at higher orders. Through any point (x, f), we can trace the characteristic curve back to its initial position (x_i, f_i) (on the outcrop line or eastern boundary). By virtue of (2.6b,c), the initial position can be calculated explicitly as

$$f_i = F_i(x,f) \equiv f\frac{1 - H_s}{1 - h_0(x,f)}, \tag{2.8a}$$

$$x_i = X_i(x,f) \equiv \frac{2f^2 w_0(f)x - h_0^2(x,f) + H_s^2}{2F_i^2(x,f)w_0(F_i)}, \tag{2.8b}$$

where h_0 is determined in (2.7). Between (x, f) and its initial position (x_i, f_i), the distance along the characteristic coordinate can be derived from (2.6a) and (2.8a) explicitly as

$$s = S(x,f) = \int_{F_i(x,f)}^{f} d\lambda/\lambda w_0(\lambda). \tag{2.8c}$$

Indeed, for the steady basic thermocline, the characteristics are isolines of potential vorticity. In the ventilated zone, they are also the streamlines.

2) The equation for linear disturbances: A decaying effect

To obtain the linear solution, we first derive its governing equation at the next order from (2.1) and (2.3),

$$h_{1t} + \mathbf{v}_{B0}\cdot\nabla h_1 + C(h_0)h_{1x} - \mu h_1 = -(1 - h_0)w_1 - \mathbf{v}_{B1}\cdot\nabla h_0, \tag{2.9a}$$

where

$$\mu \equiv \mu_a + \mu_R, \quad \mu_a = -\nabla\cdot\mathbf{v}_{B0}, \quad \mu_R = -\nabla\cdot\mathbf{C}(h_0) = -\partial_x C(h_0) = (1 - 2h_0)h_{0x}/f^2. \tag{2.9b}$$

The two terms on the right-hand side of (2.9a) are the perturbation Ekman pumping and the advection of the mean thermocline by the velocity perturbation, respectively. The right-hand side of (2.9a) is a partial linear equation, whose characteristic equations are

$$\frac{dt}{ds} = 1, \tag{2.10a}$$

$$\frac{df}{ds} = v_{B0}, \tag{2.10b}$$

$$\frac{dx}{ds} = u_{B0} + C, \tag{2.10c}$$

$$\frac{dh_1}{ds} = \mu h_1 - (1 - h_0)w_1 - \mathbf{v}_{B1}\cdot\nabla h_0, \tag{2.10d}$$

where $h_0(x, f)$ is given in (2.7a,b). Notice that the f and x equations (2.10b,c) are the same as those of the basic state [following (2.5)]. In other words, the wave rays for linear disturbances (dx/df) are the same as the characteristics of the basic state, which have been solved in (2.6a,c) or (2.8). Hence, linear waves propagate along the basic-state characteristics. This occurs because for weak perturbations, the change in the characteristics due to nonlinearity is small. However, if the perturbation becomes strong, the characteristics might be changed substantially by either the barotropic–baroclinic interaction ($\mathbf{v}_B\cdot\nabla h$) or nonlinear Rossby wave velocity ($C(h)$). These nonlinear effects will be discussed in the next section.

The initial conditions for x and f are also similar to the basic-state case. Since we only consider the forced response after the initial adjustment, the initial conditions for characteristics start either from the outcrop line $f_i = f_0$ for the ventilated zone (or the northern boundary $f_i = f_n = 1$ for the pool zone), or from the eastern boundary $x_i = 0$ for the shadow zone. The initial disturbance h_1 is set to zero for all cases, that is, $h_{1i} = 0$. Since (2.10b,c) are solved as in (2.6a,c) or (2.8), and (2.10a) is simply $t = t_i + s$, with t_i being the initial time when the characteristics starts from the outcrop line or shadow zone, the linear wave can be obtained from the linear ordinary differential equation (2.10d) alone.

Before solving the equation, let us investigate an interesting feature in (2.9a) that comes from the term $-\mu h_1$. This term is caused by the divergence of the characteristic velocity as shown in (2.9b). In the ventilated zone (VZ) [or pool zone (PZ)] with (2.7b), (2.9b) yields $\mu_R = 0$. This leads to

$$\mu = \mu_a = -\nabla\cdot\mathbf{v}_{B0} = w_0 < 0 \quad \text{in VZ or PZ}, \tag{2.11a}$$

where we have used the continuity equation for the basic state in (2.4). In the shadow zone, noting (2.7a) and (2.9b), we have $\mu_R = w_0(1/h_0 - 2)$. Combining this with (2.11a), we obtain

$$\mu = \mu_a + \mu_R = w_0 + w_0(1/h_0 - 2) = (1 - h_0)w_0/h_0 < 0. \tag{2.11b}$$

Therefore, $\mu < 0$ holds over the entire gyre. This, as suggested by (2.9a), will make a disturbance decay along a characteristic line. Physically, this occurs be-

cause, with an approximate energy flux conservation, a divergent group velocity field $\mu = -\nabla\cdot(\mathbf{v}_B + \mathbf{C}) < 0$ [see (2.9b)] implies a downstream decrease of wave energy. Equations (2.11a,b) show that this divergent group velocity is mainly caused by the divergent barotropic flow field. On shallow interfaces ($h_0 \to 0$), the divergence is strongest ($\mu_R \sim 1/h_0 \to \infty$), predominantly arising from the Rossby wave velocity field. This produces a strong decay effect on disturbances. This phenomenon occurs because of the rapid deepening of the basic thermocline near the eastern boundary on shallow interfaces.

3) THE LINEAR SOLUTION

In the absence of a mean Ekman pumping, the basic state is at rest over the whole gyre. With a mean Ekman pumping, the first significant change is the creation of a ventilated zone in the basic thermocline structure. In this zone, the advection of the subducted waters dominates while Rossby wave activity is weak. Indeed, using the Sverdrup relation $v_{B1} = fw_1$ and (2.7b), the perturbation forcing on the right-hand side of (2.9a) becomes $-(1 - h_0)w_1 - \mathbf{v}_{B1}\cdot\nabla h_0 = 0$ for $x < x_{b0}$. This zero perturbation forcing, together with the zero boundary condition in (2.9c), yields no thermocline variability in the ventilated zone, that is, $h_1 = 0$ for $x < x_{b0}$. This reflects that in the ventilated zone the perturbation Ekman pumping is mainly balanced by the perturbation density advection. It should be noted that the conclusion also applies to the pool zone on an unventilated interface because of the dominant advection there.

In the following, we will focus on the variability in the shadow zone. In the shadow zone, if the Ekman pumping (2.2a) is adopted, we find that the perturbation density advection vanishes, that is, $\mathbf{v}_{B1}\cdot\nabla h_0 = g(t)\mathbf{v}_{B0}\cdot\nabla h_0 = 0$, where we have used (2.7a). [This is true only for the form of Ekman pumping in (2.2a).] The remaining perturbation forcing is the perturbation Ekman pumping

$$-(1 - h_0)w_1 = -(1 - h_0)w_0(f)g(t).$$

To solve (2.10d), we first notice the following integral along a characteristic

$$\exp\left[-\int_0^s \mu ds\right] = \exp\left[-\int_{f_i}^{f} \frac{\mu(\lambda)d\lambda}{\lambda w_0(\lambda)}\right] = \frac{\hat{h}_0}{h_i}, \quad (2.12)$$

where $ds = df/fw_0(f)$ in (2.10b) has been used. Besides, the basic-state potential vorticity conservation (2.6b) is used to simplify the calculation because $f/(1 - h_0) = f_i/(1 - h_i)$ is constant along a characteristic. Then, (2.10d) can be integrated in the characteristic coordinate as

$$\hat{h}_1 = \hat{h}_1(s, t_i, f_i) = -\left(\frac{1}{\hat{h}_0}\right)\left(\frac{1 - \hat{h}_0}{\hat{f}}\right)\int_0^s g(t_i + \tilde{s}) \times \hat{f}(\tilde{s}, f_i)w_0(\hat{f})\hat{h}_0(\tilde{s}, f_i)d\tilde{s}, \quad (2.13)$$

where $\hat{f}$ is given in (2.6a) and $\hat{h}_0$ is the h solution in the characteristic coordinate, which can be derived from (2.6a,b) as

$$\hat{h}_0(s, f_i) = 1 - (1 - H_s)\hat{f}(s, f_i)/f_i, \quad (2.14)$$

where $h_e = H_s$ has been used. If (2.8a,c) are used, (2.13) can be expressed explicitly in (x, f) coordinate as

$$h_1 = h_1(x, f, t) = -\left(\frac{1}{h_0}\right)\left(\frac{1 - h_0}{f}\right) \times \int_0^{S(x,f)} g[t - S(x, f) + \tilde{s}]\hat{f}(\tilde{s}, F_i) \times w_0(\hat{f})\hat{h}_0(\tilde{s}, F_i)d\tilde{s}, \quad (2.15)$$

where $t_i = t - s = t - S(x, f)$ has been used. In (2.15), the second factor remains unchanged along a characteristic line because of potential vorticity conservation (2.6b). On the other hand, the first factor $1/h_0$ is caused by the decaying effect due to the divergent characteristic velocity field. Indeed, integration of the damping term along a wave ray can be seen from (2.12) as

$$\exp\left[\int_0^s \mu ds\right] = \frac{h_i}{\hat{h}_0}. \quad (2.16)$$

Along a characteristic, h_i is fixed while $\hat{h}_0$ deepens as $dh_0/ds \sim -w_0 > 0$ [see the characteristic equation of h_0 following (2.5)]. Therefore, (2.16) represents the decaying factor due to the divergent group velocity field.

The linear solution (2.15) [or (2.13)] is derived for weak perturbations $a \ll 1$. However, we will find that for an annual frequency, (2.15) agrees with the fully nonlinear solution excellently even with a strong forcing $a \sim 1$ (the perturbation forcing is comparable to the mean forcing). This point will be elaborated in later sections. Figure 1 displays an example of instantaneous zonal sections under a strong annual forcing ($\omega = 50$, $a = 0.5$). [The amplitude $a = 0.5$ has been observed for a real annual Ekman pumping field (Levitus 1988). In Fig. 1a, two instantaneous h profiles (solid lines) in September ($\omega t = 0$) and March ($\omega t = \pi$) are shown on the interface with $H_e = 0$. It is seen that the variability is weak. In Fig. 1b, the perturbations $Dh = h - h_0$ of Fig. 1a are shown (h_0 is the basic state in (2.7).] The linear solutions (in dotted lines) approximate the nonlinear solution (in solid lines) excellently. (The nonlinear solutions will be derived in the next section.) Figures 1c,d give another example for a deeper interface with $H_e = 0.6$.

c. *Thermocline evolution: Local or remote response?*

Now we analyze the thermocline evolution. To have a better understanding of the linear response, we first derive an approximate expression for the linear wave in (2.15). Integrating the characteristic form of solution in (2.13) by parts and using (2.8) (see appendix A), we obtain an approximate solution to (2.15) at $1/\omega$ order as (for $\omega \gg 1$)

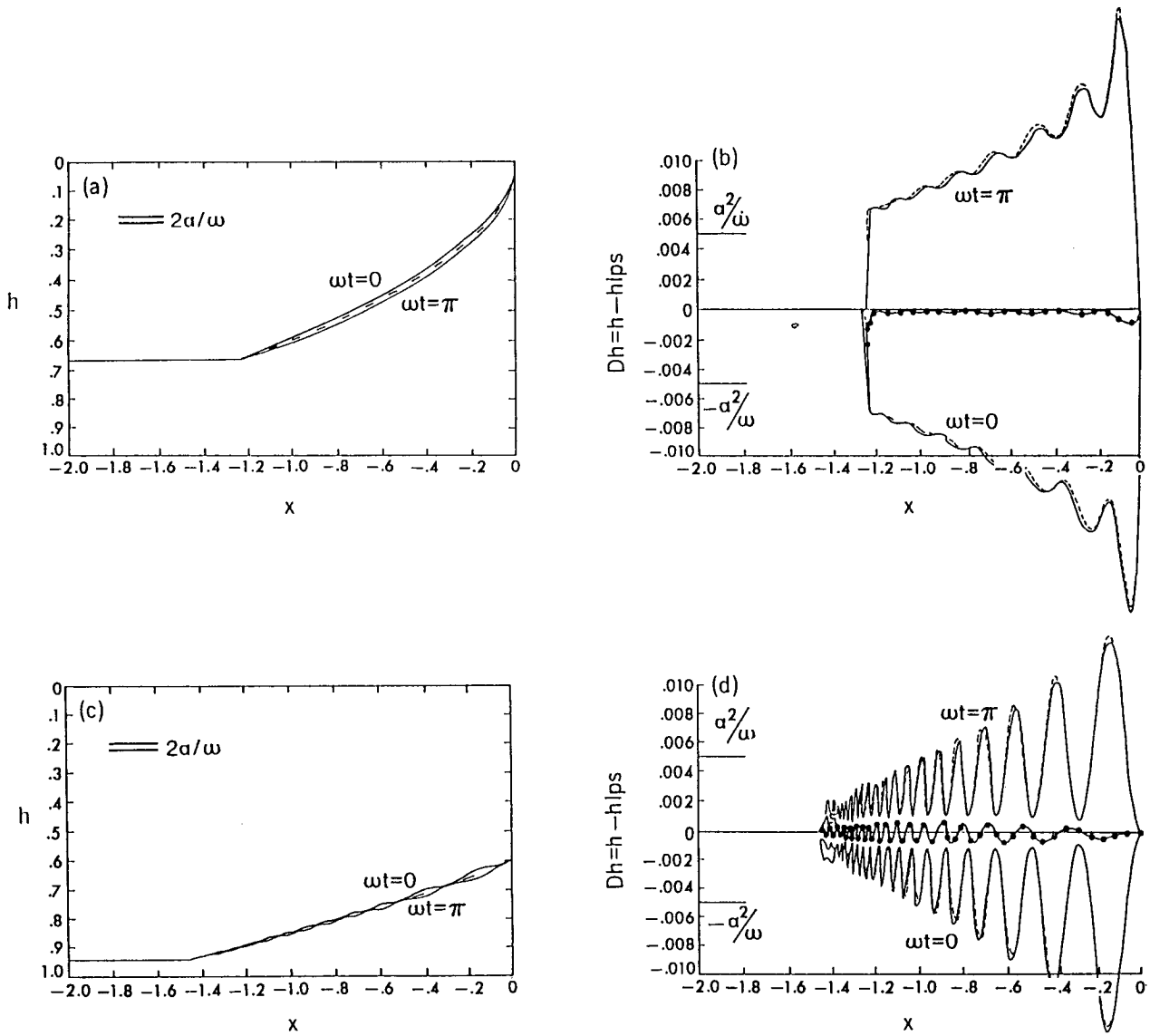

FIG. 1. Synoptic zonal sections of interfaces (a), (c) and deviations $Dh = h - h_{\text{steady}}$ (b), (d) under a strong annual Ekman pumping $\omega = 50$, $a = 0.5$. The Ekman pumping function is $w_0(f) = W_0/f$, the latitude is $f = 0.3$ and $w_0(f) = -2$: (a), (b) $H_s = 0$; (c), (d) $H_s = 0.6$. The solid lines are the nonlinear solutions. The dotted lines are linear solutions. The dashed lines are steady LPS solutions. The dot-connected lines are time-mean disturbances $\langle Dh \rangle$. One sees that the linear solution approximates the fully nonlinear solution excellently. In addition, the difference between the time-mean nonlinear solution and the steady solution forced by the time-mean Ekman pumping is very small (order 1 m), even the forcing amplitude changes half from its mean.

$$h_1 = \frac{(1 - h_0)w_0(f)}{\omega}[\cos\omega t - A\cos(\omega t - \Phi)] + O\left(\frac{1}{\omega^2}\right), \quad (2.17a)$$

where A and Φ are functions of x and f:

$$A = \frac{H_s F_i w_0(F_i)}{h_0 f w_0(f)}, \quad \Phi = \omega(t - t_i) = \omega S(x, f). \quad (2.17b)$$

Here F_i, h_0, and S are given in (2.8b), (2.7a), and (2.8c), respectively. The solution is good for high frequency when the interface is not very close to the surface (see appendix A for discussion). The first term in (2.17a) is the local response, which can be obtained by setting the advection and Rossby wave terms to zero in (2.9a), and which lags the perturbation forcing in (2.2a) by 90° in phase. The amplitude is

$$\Delta h_{\text{local}} \approx \frac{a(1 - h_0)w_0(f)}{\omega}. \quad (2.18)$$

This means that the local response decreases westward because the basic-state thermocline deepens westward. This in turn weakens the effective Ekman pumping. In comparison, the special case without a mean Ekman pumping has a flat basic thermocline interface and therefore the local response does not vary along a latitude circle.

The second term in (2.17a) is the Rossby wave, which is forced mainly along the eastern boundary where $A = 1$ (because $F_i = f$, $h_i = H_s$), and thus the eastern boundary condition $h_{1i} = 0$ is satisfied. Equation (2.17) is valid only in the shadow zone because the mean flow creates a ventilated zone that inhibits the invasion of waves from the eastern boundary.

Furthermore, the presence of a mean Ekman pumping and thermocline changes the boundary wave significantly in both its amplitude and phase. The wave amplitude decreases along a wave ray due to the divergent group velocity field. In fact, in (2.17a,b), we have the wave amplitude

$$\Delta h_{\text{wave}} \approx \frac{a(1-h_0)w_0(f)}{\omega}\frac{H_s}{h_0}\frac{F_i}{f}\frac{w_0(F_i)}{w_0(f)} = \frac{(1-h_i)aw_0(F_i)}{\omega}\exp\left(\int_0^s \mu ds\right), \quad (2.19)$$

where we have used $h_i = H_s$ and (2.16). Equation (2.19) illustrates the physics of the boundary wave elegantly. The boundary wave is excited locally at the eastern boundary by the perturbation forcing $(1-h_i)aw_0(F_i) = (1-h_i)w_1$ [see (2.12)]. This forcing produces a local response with the amplitude $(1-h_i)aw_0(F_i)/\omega$, which decays according to $\exp(\int_0^s \mu ds) = h_i/h_0$ along a characteristic line due to the divergent group velocity field. For a shallow interface ($H_s \ll 1$), the decaying effect is especially strong near the eastern boundary [see discussion after (2.11b)].

The phase Φ of the free wave, represented by the second term in (2.17a), is also changed substantially. For example, without an Ekman pumping, the phase is always in a β dispersion orientation $\Phi \sim 1/xf^2$ (in the northeast–southwest orientation) (Schopf et al. 1981). But, with an Ekman pumping, near the southern boundary of a subtropical gyre, the wave front may vary from a β dispersion (northeast–southwest) to a northwest–southeast orientation. More details about the wave front propagation are given in Liu (1991, 1993b). Here, we only need to remember that (2.17b) implies that the Φ is approximated at the leading order by $S(x,f)$.

1) Local or remote responses?

We now turn to our fundamental question of thermocline variability: whether the disturbance is caused by a local response or a remote response. Under a local response, an interface is simply forced by the perturbation Ekman pumping to move up and down with a phase lag of 90° to the forcing. On the other hand, remote responses have two mechanisms: the advection due to remotely subducted waters at the outcrop line and the eastern boundary Rossby waves.

In a ventilated zone, we have seen that the local response is as important as the remote advection and both tend to balance each other. This cancellation results in the absence of baroclinic variability.

In a shadow zone, the density advection is weak. The question then becomes the classical question: which is more important, the local response or the eastern boundary wave? Solution (2.17a) consists of a local response and a remote response. The remote response is mainly caused by the eastern boundary waves. Here A represents the relative magnitude of the boundary wave with respect to the local response; $A < 1$ gives a local response domination, while $A > 1$ gives a boundary wave domination. In the absence of a mean Ekman pumping, (2.9a) reduces to

$$\partial_t h_1 + C(H_s)h_{1x} = -w_1,$$

where $C(H_s) = -H_s(1-H_s)/f^2$ is independent of x. The solution satisfying the boundary condition in (2.9c) is easily solved as

$$h_1 = \frac{(1-H_s)w_1(f)}{\omega}\times\left[\cos(\omega t) - \cos\left(\omega t - \frac{\omega}{C(H_s)}x\right)\right].$$

A comparison with (2.17a) suggests that $A = 1$. [This can also be obtained at the limit of $w_0 \to 0$ in (2.17b).] Thus, the local response has the same magnitude as the boundary wave, that is, both are equally important.

However, with a mean circulation, it will be seen that the above conclusion no longer holds. Figures 2a,b display two examples of A (solid lines) and the boundary wave phase Φ (dashed lines) with an annual frequency $\omega = 50$. The Ekman pumping takes the form $w_e(f) = W_e(1-f)(f-f_s)$. The solution accurate to $1/\omega^2$ in appendix A is used. Figure 2a is on a shallow interface ($H_s = 0.1$), while Fig. 2b is on a deep interface ($H_s = 0.5$). Two features are salient. First, local responses tend to dominate on the shallow interface, while boundary waves dominate on the deep interface. Secondly, local responses are stronger in the northern part of an interface, while boundary waves are stronger in the southern part. These two features are also clear for decadal forcings. In fact, at the leading order, the relative amplitude A in (2.17b) is independent of frequency.

To understand the physics of these two features, we rewrite the relative amplitude A in (2.17b) as

$$A = \left[\frac{H_s}{h_0}\right]\left[\frac{(1-H_s)w_0(F_i)}{(1-h_0)w_0(f)}\right] > 0. \quad (2.20)$$

Toward the interior, the divergent group velocity produces the eastern boundary Rossby waves decaying toward the interior (the first factor), resulting in a weaker

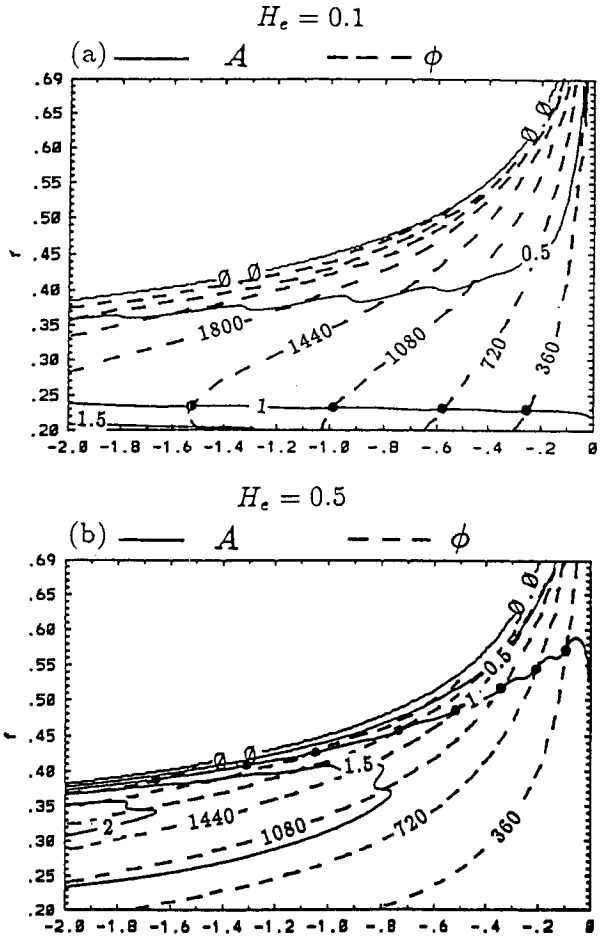

FIG. 2. Here, A is the relative amplitude of the eastern boundary Rossby to that of the local response; Φ is the phase of the boundary waves of linear solutions of second-order approximation $O(1/\omega^2)$ in (A.1). The Ekman pumping has the form $w_0(f) = W_0(1-f)(f-f_s)$ and its amplitude is such that $w_0(f)|_{f=0.5(1+f_s)} = -1$. The outcrop line is at $f_0 = 0.9$, (but the figure does not show all the interface). The frequency is annual, $\omega = 50$. Panel (a) is on a shallow interface with the eastern boundary interface $H_s = 0.1$. A large area of $A < 1$ is present and thus local response dominates. Panel (b) is on a deep interface with $H_s = 0.5$. The $A > 1$ area occupies most of the domain. Thus, remote Rossby waves are more important.

boundary wave response. In contrast, a westward-deepening basic thermocline produces a smaller effective Ekman pumping (the second factor), in favor of a weaker local response. Therefore, which effect is important depends on the competition between the two mechanisms. On a shallow interface, the divergent Rossby wave velocity is extremely strong [see discussion following (2.11b)], suppressing the eastern boundary wave significantly. Therefore, the local response is dominant. The opposite occurs for a deeper interface, where the boundary wave tends to dominate.

In addition, a Rossby wave is produced at latitude F_i and then propagates southward, requiring $F_i > f$. In the northern part of a subtropical gyre, $|w_0(f)|$ decreases poleward. Thus, $w_0(F_i)/w_0(f) < 1$, implying a relative weak boundary wave. Physically, in the northern part, the local Ekman pumping $w_0(f)$ is stronger than the Ekman pumping $w_0(F_i)$ that generates boundary waves along the eastern boundary. Therefore, the local response tends to be stronger. The opposite occurs in the southern part of the gyre. In particular, near the southern boundary, where local Ekman pumping vanishes, $w_0(f) \to 0$, the boundary waves are forced in the middle of the gyre where $w_0(F_i)$ is finite. Thus, $w_0(F_i)/w_0(f) \to \infty$, implying a dominant boundary wave effect.

2) VARIABILITY OF THERMOCLINE STRUCTURE AND CIRCULATION

Figure 3a depicts the disturbance ah_1 under a strong annual forcing $a = 0.5$, $\omega = 50$ in September ($\omega t = 0$), December ($\omega t = 90°$), March ($\omega t = 180°$), and June ($\omega t = 270°$). The eastern boundary depth is $H_s = 0.1$ (as in Fig. 2a). It is seen that the disturbance reaches about maximum in March and reaches the negative maximum in September, which is typical for local response dominance. The maximum amplitude is about 0.01, corresponding to a dimensional depth of about 6 m (if the total depth $H = 600$ m). Figure 4 displays ah_1 with a weak decadal forcing $\omega = 5$, $a = 0.05$. A positive (negative) Rossby wave anomaly is formed near the eastern boundary during winter (summer). Then, the anomaly propagates and intensifies westward to occupy the interior during fall (spring).

Last, we observe the circulation. Figures 3b,c illustrate the upper- and lower-layer circulation for the thermocline disturbance in Fig. 3a. The upper-layer circulation remains to be an anticyclonic gyre. This gyre reaches its maximum strength in the winter and its minimum in the summer. The lower layer is more interesting. A penetration of water toward the shadow zone appears in the winter when the wind is strong (similar to a spinup process in LIU Fig. 6). In contrast, in the summer when the wind is weak, the lower layer exhibits a northward flow and a cyclonic gyre in the shadow zone, while the anticyclonic gyre is confined in the nothern part of the ventilated zone. (This agrees with the circulation during a spindown process in LIU Fig. 7.) Physically, the changing of flow is caused by the barotropic response to the changing wind (see LIU for details). This seasonal reversal of flow direction has been observed in some numerical modelings of the southeastern part of the North Pacific (Spall 1991, personal communication). The wavy structure is barely seen, consistent with the weak thermocline variability.

To summarize, the mean thermocline structure influences disturbances significantly. First, the divergent group velocity results in a decay of Rossby waves. Second, a ventilated zone is created where Rossby waves from the eastern boundary are prohibited. Third, in a shadow zone, the thermocline variability is dominated by local response on shallow interfaces but is dominated by Rossby waves on deeper interfaces.

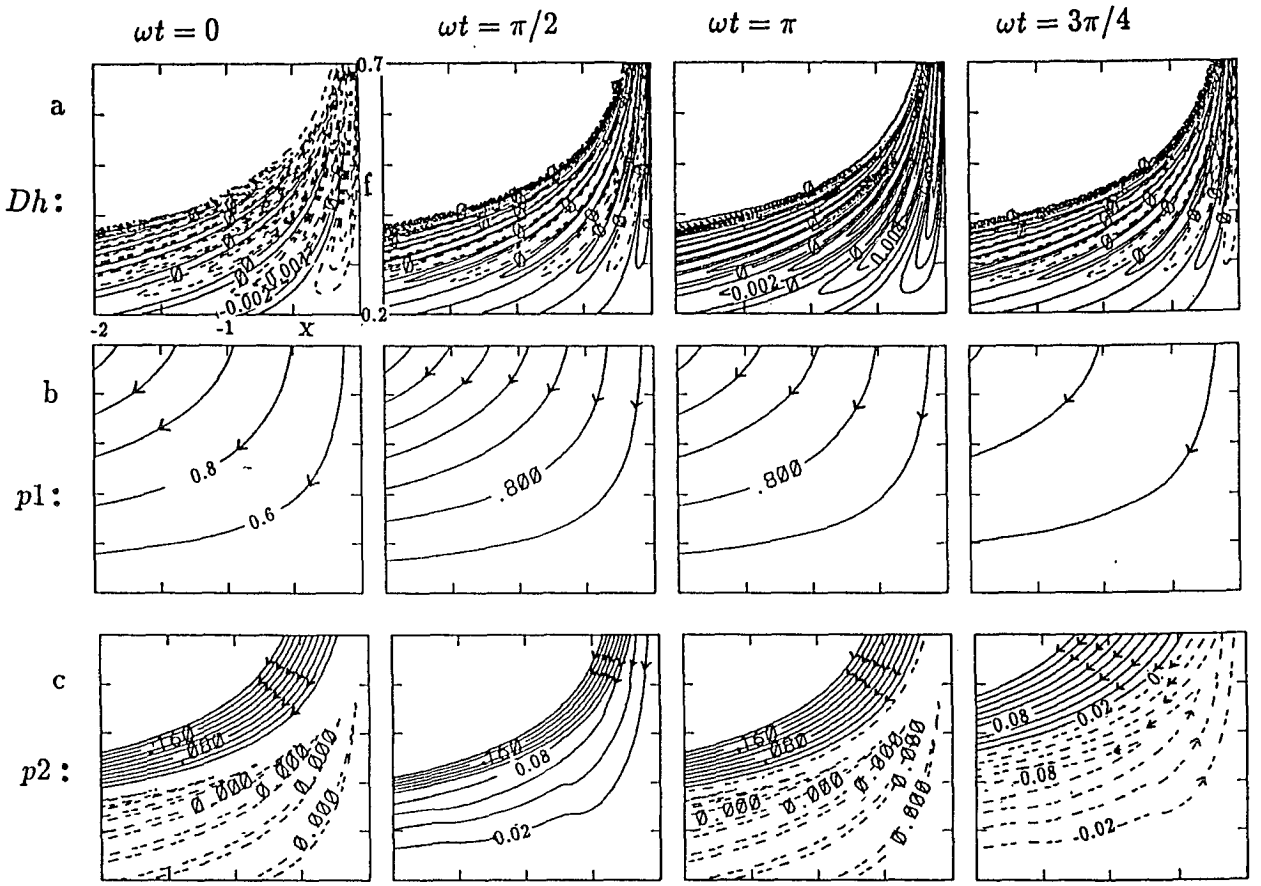

FIG. 3. The two-dimensional structures of the linear solution of a shallow interface $H_s = 0.1$ with a strong annual forcing $\omega = 50$, $a = 0.5$ (corresponding to Fig. 2); w_e is parabolic as in Fig. 2. (a) Disturbance Dh in September ($\omega t = 0$), December ($\omega t = \pi/2$), March ($\omega t = \pi$), and June ($\omega t = 3\pi/2$), consecutively. (b) Upper-layer pressures for four seasons. (c) Lower-layer pressures for four seasons with arrows representing flow direction. In (c), the contours only draw pressure with $p_2 < 0.2$. As a result, the flow in most of the ventilated zone is not shown. The seasonal reversal of flow in the shadow zone is obvious.

3. Nonlinear theory

Now we investigate the nonlinear thermocline. A comparison between linear and nonlinear solutions will also be carried out. It will be seen that under a strong decadal forcing, linear solutions fail to capture some important features of the nonlinear solution. Finally, we analyze the time-mean structure of the nonlinear thermocline.

a. The nonlinear solution

We seek solutions of the nonlinear equation (2.1a). The characteristic equations are

$$\frac{dt}{ds} = 1,$$

$$\frac{df}{ds} = f w_e(f, t),$$

$$\frac{dh}{ds} = -(1 - h) w_e(f, t),$$

$$\frac{dx}{ds} = -[f^2 w_e(f, t) x]_f / f - h(1 - h)/f^2.$$

Similar to the approach of obtaining (2.6) from the basic-state characteristic equations of (2.5), with the Ekman pumping in (2.2a), the characteristic equations of (2.1) can be solved to yield parametric solutions:

$$t = t_i + s, \tag{3.1a}$$

$$\int (f/f_i) d\lambda / \lambda w_0(\lambda) = s - \frac{a}{\omega}(\cos\omega t - \cos\omega t_i),$$

$$\text{or implicitly} \quad f = \hat{f}(s, t_i, f_i), \tag{3.1b}$$

$$f/(1 - h) = f_i/(1 - h_i) \quad \text{or} \quad h = \hat{h}(s, t_i, f_i), \tag{3.1c}$$

$$x f^2 w_0(f) = x_i f_i^2 w_0(f_i) - \frac{1 - h_i}{f_i} \int_0^s [1 - (1 - h_i)\hat{f}/f_i] \hat{f} w_0(\hat{f}) ds,$$

$$\text{or} \quad x = \hat{x}(s, t_i, f_i, x_i). \tag{3.1d}$$

Again, here the quantities with carets represent the solution in the characteristic coordinate. Similar to the basic-state case, for forced solutions, the initial con-

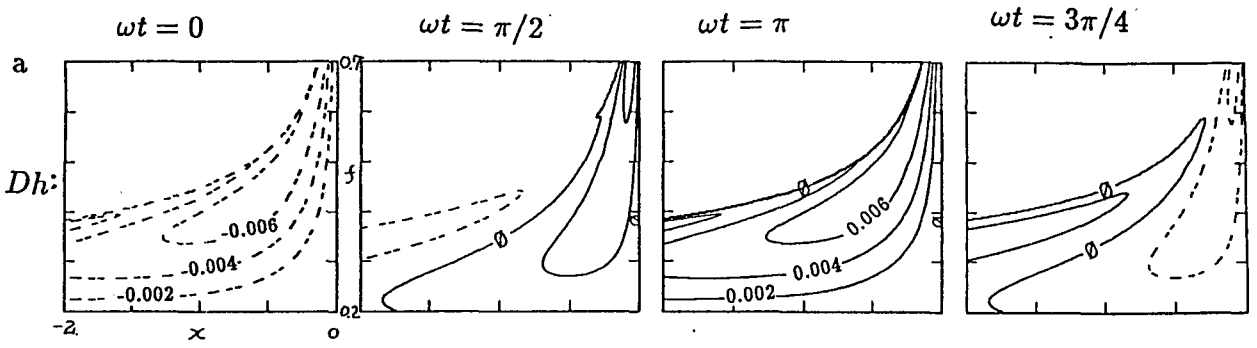

FIG. 4. The 2D structure of the disturbance Dh during four seasons for linear solutions under a weak decadal forcing with $\omega = 5$, $a = 0.05$. The Ekman pumping is parabolic as in Fig. 2. The interface is a shallow interface with $H_s = 0.1$. One sees that the disturbance propagates westward and deforms.

ditions for characteristics in the ventilated (or pool) zone and shadow zone, respectively, come from the outcrop line and the eastern boundary; that is,

$$f_i = f_0, \quad h_i = H_s \text{ in the VZ } (f_0 < 1) \text{ or PZ } (f_0 = 1), \tag{3.2a}$$

$$x_i = 0, \quad h_i = H_s \text{ in the SZ.} \tag{3.2b}$$

An example is the case with $w_0(f) = W_0/f$. All nonlinear solutions in this paper have this Ekman pumping (except for Fig. 7)[2] because this Ekman pumping enables us to integrate (3.1b,d) explicitly as

$$\hat{f} = f_i + W_0\left[s - \frac{a}{\omega}(\cos\omega t - \cos\omega t_i)\right], \tag{3.3a}$$

$$x\hat{f} = x_i f_i - \frac{h_i(1-h_i)}{f_i}s + \frac{(1-h_i)^2 W_0}{f_i^2} \times \left[\frac{s^2}{2} + \frac{as}{\omega}\cos\omega t_i - \frac{a}{\omega^2}(\sin\omega t - \sin\omega t_i)\right]. \tag{3.3b}$$

In principle, from (3.1) and (3.2), one should be able to obtain an explicit solution of the form

$$h = h(x, f, t). \tag{3.4}$$

It can be shown that the general solution (3.4) possesses the primary period $T = 2\pi/\omega$. This periodicity ensures that the primary frequency ω is the lowest nonzero frequency of the forced thermocline. In other words, no subharmonics will be produced except for, perhaps, the time-mean component. Mathematically, the periodicity enables a Fourier series to be used to decompose the time series of the nonlinear thermocline solution.

[2] This Ekman pumping resembles the middle part of a subtropic gyre fairly well, although it obviously fails to represent the region near the southern and northern boundaries because the boundaries are absent. This Ekman pumping is used in this paper to study the variability along zonal sections resembling those in the middle part of a subtropical gyre.

We now derive solutions in the ventilated (or pool) zone and shadow zone. In the ventilated (or pool) zone, (3.1c) and (3.2a) yield the solution

$$h = 1 - (1 - H_s)f/f_0, \quad x < x_b(f, t). \tag{3.5}$$

The ventilated (or pool) zone is a uniform potential vorticity pool with the constant potential vorticity $f_0/(1 - H_s)$. Therefore, no matter how strong and what pattern the Ekman pumping is, there is no thermocline variability. (This has been discussed in the previous section for linear waves.) This is so because only the potential vorticity conservation is used in (3.5). Under a zonal outcrop line (or a constant interface depth $H_s > 0$ at the northern boundary when $f_0 = f_n$), the potential vorticity is always uniform, and hence there is no variability.

In the shadow zone, (3.1) and (3.2b) yield

$$t = t_i + s, \tag{3.6a}$$

$$f = \hat{f}(s, t_i, f_i), \tag{3.6b}$$

$$h = 1 - (1 - H_s)f/f_i, \tag{3.6c}$$

$$x\hat{f}^2 w_0(\hat{f}) = -\frac{1 - H_s}{f_i}\int_0^s [1 - (1 - H_s)\hat{f}/f_i] \times \hat{f} w_0(\hat{f})\, ds, \quad x > x_b(f, t). \tag{3.6d}$$

In (3.5) and (3.6), x_b is the shadow zone boundary that is formed by characteristics initiating from $(0, f_0)$ at successive times; x_b varies with time and is determined parametrically from (3.6b,d) as

$$f_b = \hat{f}(t - t_i, t_i, f_0), \quad x_b = -\frac{1 - H_s}{f_0 f_b^2 w_0(f_b)} \times \int_0^{t-t_i} [1 - (1 - H_s)\hat{f}/f_0]\hat{f} w_0(\hat{f})\, ds. \tag{3.7}$$

This shadow zone boundary will sweep back and forth as the Ekman pumping varies (also see LIU for the wave front B). Two examples of (3.7) are presented in Fig. 5. Following LIU, we call the region through

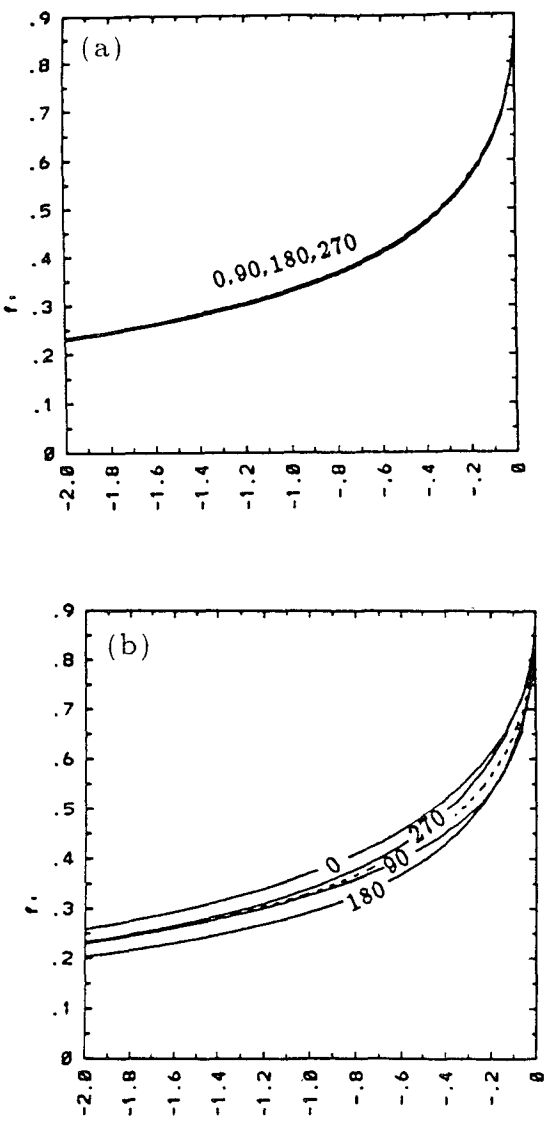

FIG. 5. The instantaneous shadow zone boundaries at four seasons (labeled by the phase ωt; corresponding to the alternative zone in the text). The Ekman pumping takes the form of Fig. 1 and $H_s = 0$. The dashed lines are the shadow zone boundary x_{B0} of the steady thermocline under the mean Ekman pumping. (a) Under a strong annual forcing $\omega = 50$ and $a = 0.5$. The boundary moves little. (b) Same as (a) except for $\omega = 5$. Now, the migration of the boundary is much larger than the annual case, but it still occupies a small portion of the basin.

which x_b passes the "alternative zone" because this region is alternately occupied by an instantaneous ventilated zone and shadow zone. Figure 5a shows that the annual forcing case has a very narrow alternative zone, even with a strong perturbation ($a = 0.5$). This occurs because the shadow zone boundary is mainly controlled by the baroclinic Rossby waves, which develop very little within one annual period. Even with a strong decadal forcing in Fig. 5b, the alternative zone is not large, although it could occupy a fairly large portion of a zonal section in the southern part of a gyre. However, it is interesting to point out that the wave rays (or the characteristics) starting at different times vary much more strongly than the x_b itself. This implies that the wave energy path under a varying Ekman pumping can deviate significantly from the steady ray calculated in a steady model with the time-mean Ekman pumping.

b. Time-mean thermocline

The thermocline equation (2.1a) includes two nonlinear effects: the interaction between the barotropic and baroclinic flows ($\mathbf{v}_B \cdot \nabla h$) and the nonlinear Rossby wave effect [$C(h)$]. The former has been studied by Dewar (1989) in a QG model under an annual forcing, while the latter was first explored by Anderson and Killworth (1979) in a 1½-layer model. With this nonlinearity under a periodic Ekman pumping, one should expect a time-mean thermocline $\langle h \rangle$ differing from the steady thermocline h_0 that is forced by the time-mean Ekman pumping $\langle w_e \rangle = w_0$. (Without confusion, hereafter, this steady thermocline is simply called the steady thermocline.) Here, we will investigate the time-mean thermocline.

With a strong annual forcing (as used in Fig. 1), one has seen that the instantaneous disturbance $Dh = h - h_0$ is at the order of a/ω, that is,

$$Dh \leqslant O\left(\frac{a}{\omega}\right). \tag{3.8}$$

The nondimensional maximum is about 0.01, which corresponds to a dimensional depth of about 6 m (if the total depth is about 600 m). In addition, the time-mean disturbance $\langle Dh \rangle = \langle h - h_0 \rangle = \langle h \rangle - h_0$ (dot-connected lines in Fig. 1: b,d,f) is not zero. The mean disturbance is no larger than a^2/ω, or

$$\langle Dh \rangle \leqslant O\left(\frac{a^2}{\omega}\right). \tag{3.9}$$

The nondimensional maximum is less than 0.001 or a dimensional depth of less than about 0.6 m. Thus, $\langle Dh \rangle$ is small compared with the instantaneous disturbance Dh for either a high frequency or a weak decadal frequency forcing $a \ll 1$. Nevertheless, it is interesting to observe a slightly negative $\langle Dh \rangle$ component along the whole section, implying a shallower mean thermocline than the steady one. At a decadal frequency, if the forcing amplitude becomes strong, (3.8) and (3.9) suggest that $\langle Dh \rangle$ may increase rapidly compared with Dh. This phenomenon is seen clearly in Fig. 6, which plots an example at the latitude $f = 0.3$ with a strong decadal forcing $\omega = 5$, $a = 0.5$; the Ekman pumping $w_e = W_0/f$ is used. Figure 6b shows a ventilated case ($H_s = 0$). One sees that $\langle Dh \rangle$ can reach about one-third of Dh. In addition, a salient feature is the strong negative $\langle Dh \rangle$ along the whole zonal section, implying a time-mean interface shallower than the steady one. We will return to this mechanism later. A

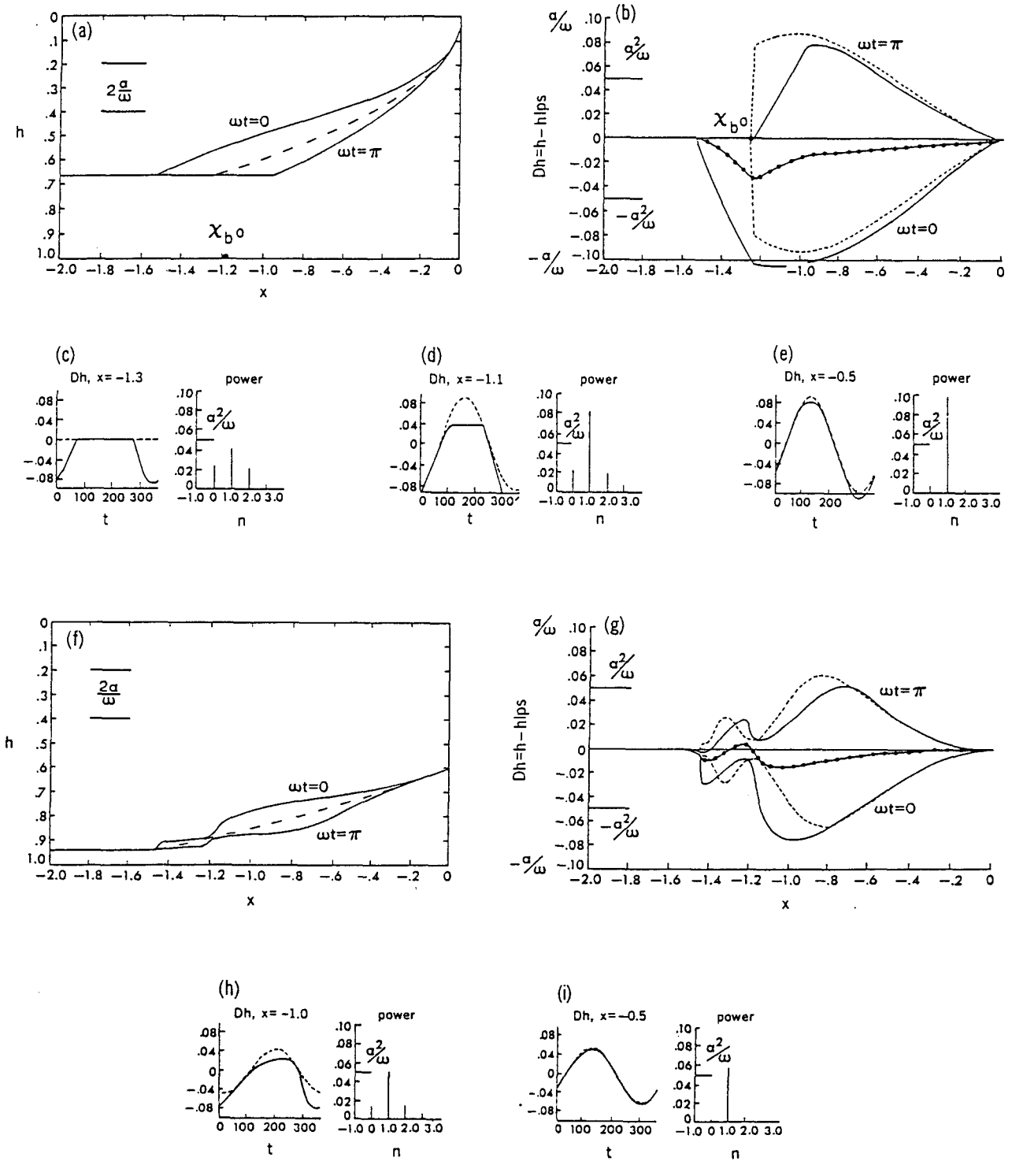

FIG. 6. Zonal sections, time series of local interfaces, and their Fourier components of nonlinear solutions under a strong decadal Ekman pumping $\omega = 5$, $a = 0.5$. The Ekman pumping has the same form as in Fig. 1. (a), (b), (f), and (g) Same as in Figs. 1a–d, respectively, except for $\omega = 5$, $a = 0.5$. (c), (d), and (e) The local time series of Dh and their Fourier components at three locations in (a) and (b). For the Fourier components, the abscissa n refers to the frequency $n\omega$. (h) and (i) Two time series of Dh and Fourier components at two points in (f) and (g). Compared with Fig. 1, the linear solution differs from the nonlinear solution significantly in the western part of the shadow zone, where the time-mean solution is shallower than the steady solution under the time-mean Ekman pumping on the order of 10 m. There, the time series show that the nonlinearity mainly creates the zero and second harmonics. In other parts, the linear solution is still fairly good.

common character of ventilated interfaces (in Fig. 1b and Fig. 6b) is that $\langle Dh \rangle$ achieves its maximum amplitude in the alternative zone, which is located in the western flank of the shadow zone. Figure 6g shows an unventilated interface with $H_s = 0.6$. One sees that even on this interface, $\langle Dh \rangle$ still reaches its maximum in the western shadow zone. In Fig. 6, the nondimensional maximum $\langle Dh \rangle$ ranges from -0.02 to -0.04 at different depths, corresponding to a dimensional mean deviation of -12 to -24 m. In addition, in the region where $\langle Dh \rangle$ is strong, the linear solution deviates from the nonlinear solution significantly. In contrast, in the eastern part of the shadow zone where $\langle Dh \rangle$ is always weak, it is surprising to see how well the linear solution resembles its nonlinear solution in all the cases.

Some time series of local interface variations and their Fourier components are also shown. Figure 6e is located in the eastern part of the shadow zone of the ventilated interface in Figs. 6a,b. The number on the abscissa, n, corresponds to the frequency $n\omega$. The primary component (with the primary frequency ω) dominates, while other components are negligible. Figure 6i gives another example in the eastern shadow zone. The Fourier components are similar to Fig. 6e. A strikingly different behavior appears in the alternative zone on a ventilated interface (Figs. 6c,d) and (somewhat less strikingly) in the western part of the shadow zone (Fig. 6h). Now, both the time-mean component and the second superharmonics (with frequency 2ω) become rather strong. In addition, observing all the Fourier components of these time series, one sees that the time-mean component is about the same magnitude as the second superharmonic component, while other higher superharmonics are negligible. We will return to this point later.

With a strong decadal forcing ($\omega = 5$, $a = 0.5$), Fig. 7a displays the horizontal structure of the time-mean thermocline disturbance $\langle Dh \rangle$ for a parabolic form $w_0(f) = W_0(1-f)(f-f_s)$ of Ekman pumping on a ventilated interface. The solution is found by first solving the characteristic equations in (2.1a) using the fourth-order Runge–Kutta method at each time. Then the solution is mapped objectively onto regular grids. Finally, the time mean is carried out at each grid point. One sees that $\langle Dh \rangle$ has a negative component within the entire shadow zone. The strongest mean deviation occurs within the alternative zone. The nondimensional maximum mean deviation is about -0.03 or dimensionally -18 m. The instantaneous patterns in four seasons (not shown) are similar to that in Fig. 4 except now the alternative zone is much larger. Using this time-mean thermocline, the corresponding lower-layer pressure (or streamfunction) is shown in Fig. 7b. There is a strong southward flow in the alternative zone, which weakens toward the east. This southward mean flow corresponds to a mean vertical downwelling inside the shadow zone (not shown). As a result, in the time-mean thermocline, the lower-layer fluid in the shadow zone is no longer motionless. Instead, it has a mean southward flow.

In comparison, an annual forcing produces a very different $\langle Dh \rangle$ as shown in Fig. 7c. The mean disturbance is much weaker (note the different contour intervals) than the decadal case in Fig. 7a. The dimensional maximum value is about ± 1 m. In addition, the pattern exhibits alternative highs and lows. In the mean lower-layer pressure field of Fig. 7d, these highs and lows correspond to some microgyres, as found by Dewar (1989). In the previous example in Fig. 1a, these alternate highs and lows are also obvious in the mean zonal profile (dot-connected line).

c. *Mechanisms for the mean thermocline*

Now we analyze the mechanism for the time-mean thermocline structure. It turns out that in different regions and for different frequencies, the mechanisms are different. Here, we concentrate on the shadow zone for low-frequency cases and the shallower mean thermocline structure.

In the shadow zone (east of the alternative zone on a ventilated interface, or the whole unventilated zone), the main mechanism is the nonlinearity of the Rossby wave that is to be explained in the following. Consider an even simpler model—a 1½-layer model. The upper-layer depth is determined by

$$h_t + C(h)h_x = -w_e(f, t), \qquad (3.10)$$

where $C(h) = -h/f^2$. The only nonlinear effect in this model is the nonlinear Rossby wave. It can be proven that the solution in (3.10) is periodic if $w_e(f, t)$ is periodic in time. Thus, averaging (3.10) over one period and then integrating it along the x direction, we obtain the energy equation:

$$\langle h^2 \rangle = h_0^2 = 2f^2 w_0(f)x + H_s^2, \qquad (3.11)$$

where h_0 is the steady thermocline [as in (2.7a)] forced by the time-mean Ekman pumping $\langle w_e(f, t) \rangle = w_0(f)$. Decomposing the thermocline into the time-mean and perturbation parts as $h = \langle h \rangle + h'$, (3.11) becomes

$$\langle h \rangle^2 + \langle h' \rangle^2 = h_0^2, \quad \text{or}$$

$$\langle h \rangle^2 - h_0^2 = -\langle h' \rangle^2 < 0. \qquad (3.12)$$

This states that the mean thermocline is always shallower than the steady thermocline. Physically, (3.11) and (3.12) suggest that part of the input mean available potential energy leaks away as disturbance potential energy due to the nonlinear Rossby wave.

The preceding argument also applies to our two-layer model if the forcing frequency is low. Indeed, when the forcing frequency approaches zero, both the local variability (h_t) and density advection ($\mathbf{v}_B \cdot \nabla h$) should diminish (when $\omega = 0$, both of them vanish

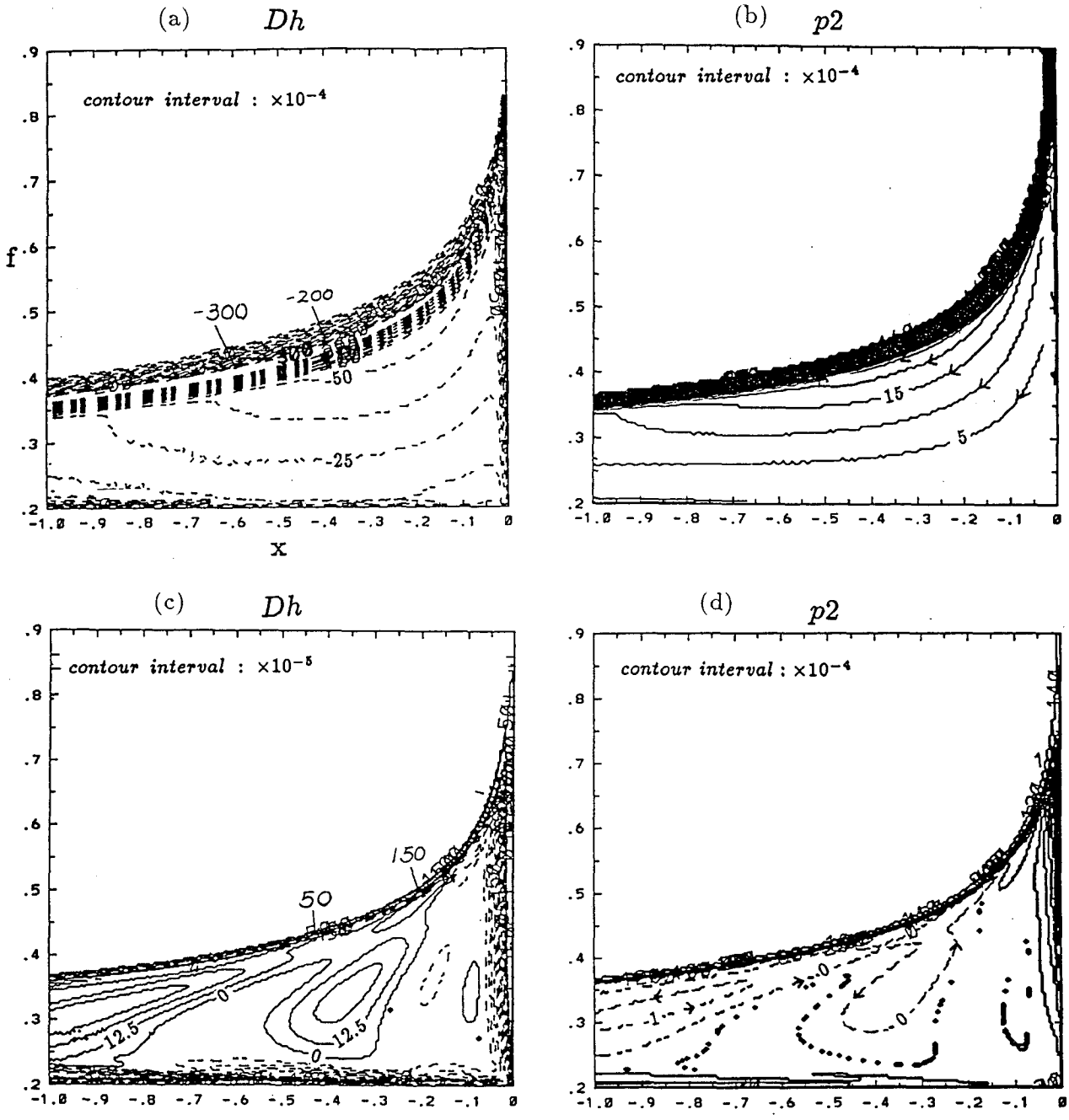

FIG. 7. The 2D time-mean structures of nonlinear solutions under the Ekman pumping $w_0(f) = W_0(1 - f)(f - f_s)$ with $w_0(f)|_{f=0.5(1+f_s)} = -2$. The solution is obtained by integrating the characteristic equations of (1.7a) using a fourth-order Runge–Kutta method at each time. Then the values are objectively mapped onto regular grids and averaged. (a), (b) Shows $\langle Dh \rangle$ and the corresponding lower-layer pressure p_2 (or streamline) for a strong decadal forcing $\omega = 5$, $a = 0.5$. (c) and (d) The same as (a) and (b) except for an annual forcing $\omega = 50$. The mean lower-layer pressure contours are chosen such that the flow field in the shadow zone can be seen clearly. As a result, the flow within most of the ventilated zone is not shown. In the annual case, the time-mean solution is weak in the shadow zone and the deviation from the steady solution alternates in space to form microgyres (Dewar 1989). In the decadal case, however, the mean solution is always shallower than the steady solution.

exactly in the shadow zone). Thus, the major dynamic balance of (3.1) degenerates to $C(h)h_x \approx -(1 - h)w_e(f, t)$, where $C(h) = -h(1 - h)/f^2$. This dynamic balance leads to the energy equation similar to (3.12):

$$h^2 \approx 2f^2 w_e(f, t)x + H_s^2 \qquad (3.13)$$

for *very low* frequency. This is the Sverdrup relation with time as a parameter. Averaging (3.13) will give rise to the same relation as (3.11) or (3.12). With the

Ekman pumping in (2.2a), we can estimate the mean deviation $\langle Dh \rangle$:

$$\begin{aligned}\langle Dh \rangle &\equiv \langle h \rangle - h_0 \\ &= \langle \sqrt{2f^2 w_0(f)(1 + a\sin\omega t)x + H_s^2} \rangle \\ &\quad - \sqrt{2f^2 w_0(f)x + H_s^2} \\ &= -h_0 \langle 1 - \sqrt{1 + a(1 - H_s^2/h_0^2)\sin\omega t} \rangle < 0 \\ &\qquad \text{for} \quad 0 < a < 1. \quad (3.14a)\end{aligned}$$

For a weak forcing $a \ll 1$, (3.14a) can be approximated as

$$\langle Dh \rangle \approx -\frac{a^2}{16}(1 - H_s^2/h_0^2)^2 h_0. \quad (3.14b)$$

Quantitatively, in Fig. 6 or Fig. 7a ($a = 0.5$, $h_0 \approx 500$ m, and $H_s/h_0 \ll 1$), this gives about 10 m (or a nondimensional value 0.017), agreeing with the maximum $\langle Dh \rangle$ in the shadow zone (not in the alternative zone!). In fact, calculations show that (3.14b) gives a good approximation to (3.14a) until $a = 1$. Therefore, in a shadow zone, the time-mean disturbance seems to have the upper bound at low frequency (by letting $a \to 1$ and $H_s \to 0$)

$$\frac{\langle Dh \rangle}{h_0} \leq O\left(\frac{1}{16}\right). \quad (3.15)$$

In addition, since h_0 deepens westward, (3.14b) suggests that $\langle Dh \rangle$ also increases westward. In the eastern part of the shadow zone, this westward increasing mean deviation can be observed clearly in Figs. 6b,g. However, $\langle Dh \rangle$ increases toward the west only to about a quarter of the wavelength as seen in Figs. 6b,g. This differs from (3.14) because (3.14) is valid only when $\omega \to 0$ (and the wavelength goes to infinity).

With a high frequency, the advection term becomes dominate, a response for the microgyres in the mean thermocline (appendix B). In the alternative zone, the alternate of the Rossby wave and cold advection is very efficient in producing a very shallow mean thermocline. [See appendix B, chapter 3, of Liu (1991).]

Last, we point out that (3.13) [or (B.1) for a high-frequency case] shows that the time-mean component has the same amplitude as the second harmonics, which has been seen in the previous examples in Fig. 6. This spectrum is characterized by both a rapid rise and a rapid decrease of the local interface variability. This is different from that forced by a periodic surface temperature (Liu and Pedlosky 1993).

4. Thermocline variability under a variable Ekman pumping

Finally, we investigate the variability with different frequency and amplitude of forcing. In particular, we are interested in how important the nonlinear effect is. Visually, the examples in Fig. 1 indicate that the linear solutions are able to represent the nonlinear solutions excellently along the whole zonal section with a strong annual forcing. If the amplitude of the decadal forcing becomes strong, Fig. 6 illustrates that the linear solution still approximates the nonlinear solution well in the eastern part of the shadow zone, but it fails in the western part of the shadow zone and the alternative zone.

As a further step to studying the variability and its nonlinearity under different amplitude and frequency of forcing, we examine the variability of the zonally integrated interface disturbance

$$\frac{1}{x_b}\int_0^{x_b} Dh\,dx, \quad (4.1)$$

where x_b is the instantaneous shadow zone boundary in (3.7). Subject to various forcing amplitudes a and frequencies ω, for the zonally averaged variability (4.1), the amplitude of the primary component is depicted in Fig. 8a. The Ekman pumping is chosen to be $w_e = W_0/f$. Qualitatively, the amplitudes of the primary component agree with the linear solutions (2.17) or (A.1). For high frequencies (higher than decadal), their

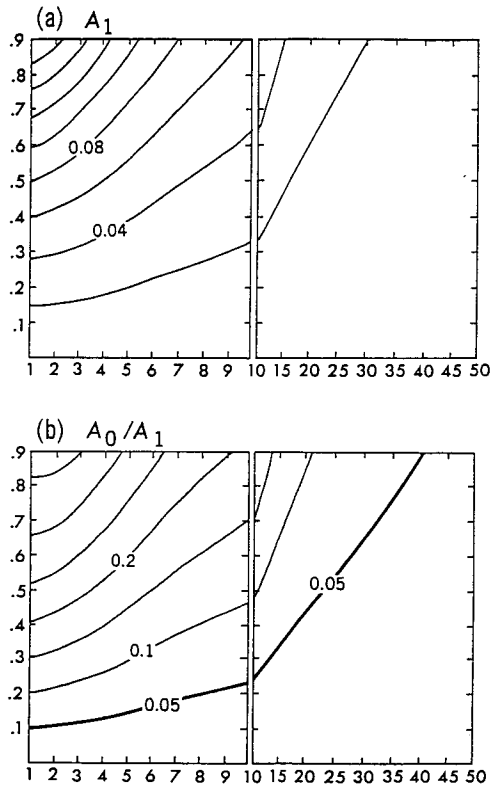

FIG. 8. Thermocline variability of the zonally integrated disturbance (4.1) subject to different forcing frequency ω and amplitude a. The Ekman pumping takes the same form as in Fig. 1. Here $H_s = 0$ is adopted. (a) The primary component A_1; (b) ratio of the time-mean component to the primary component A_0/A_1. The line of ratio value 0.05 is darkened, which separates the parameter region where nonlinearity is negligible (toward higher frequency and smaller amplitude direction) from those where nonlinearity is not negligible.

amplitudes are proportional to a/ω (straight lines in the $\omega-a$ plane passing through the origin). As frequencies approach zero, the amplitudes approach finite limits because of the finite width of the basin.

To analyze the nonlinearity quantitatively, we decompose the time series in (4.1) into a Fourier series $\int_0^{x_b} Dhdx/x_b = \sum_{n=0}^{\infty} A_n \sin(n\omega t - \theta)$. Then, we can judge the importance of the nonlinearity by the power ratio between the sum of all sub- and superharmonics (which are generated by nonlinearity) and the primary component, that is, $P_{\text{ratio}} = (\sum_{n\neq 1} A_n^2/A_1^2)^{1/2}$. Since we have seen that the powers of the second superharmonics A_2 and the time-mean component A_0 are about the same while other components are negligible, the power ratio can be approximated as $P_{\text{ratio}} \approx 2A_0/A_1$. In Fig. 8a A_0 has been shown; the ratio A_0/A_1 is shown in Fig. 8b. The contour $A_0/A_1 = 0.05$ (heavy solid line in Fig. 8d) can be taken as the criterion for $P_{\text{ratio}} = 0.1$ in the $\omega - a$ plane. Below this line the power ratio is less than 0.1 and the total power of the nonlinearly generated harmonics is one order less than that of the primary component. In other words, nonlinearity is negligible. This regime is the linear regime and mainly consists of weak decadal forcing and strong annual forcings (e.g., the examples in Fig. 1). Above the $P_{\text{ratio}} = 0.1$ line the nonlinearly generated components are no longer negligible. The regime consists of strong decadal forcing and is called the nonlinear regime. (It is perhaps more proper to call it the weakly nonlinear regime because the nonlinearity is not dominant.) Figure 6 is an example of this nonlinear regime. For the parameters in Fig. 6 ($\omega = 5$, $a = 0.5$), we find from Fig. 8d that $A_0/A_1 \approx 0.17$. Equation (4.2) then suggests that $P_{\text{ratio}} \approx 0.34$. This means that about 30% of the energy of this decadal forcing is transferred nonlinearly to the time-mean and higher components. It should be born in mind that the zonally averaged disturbance (4.1) underestimates the maximum local nonlinearity in the western shadow zone or the alternative zone.

5. Summary

As an extension of the spinup study of a ventilated thermocline of LIU, the two-layer planetary geostrophic model is used to investigate the thermocline variability under a variable Ekman pumping. The features found in the spinup and spindown also exist in the periodic Ekman pumping case, with the seasons of an increasing and a decreasing Ekman pumping resembling the spinup and spindown, respectively. This is particularly true for annual forcings (i.e., with periods comparable to one year). Therefore, under a varying Ekman pumping, the thermocline variability is much stronger in the shadow zone than in the ventilated zone. The direction of the lower-layer circulation in the shadow zone oscillates southward and northward. During a season when w_e intensifies, the lower-layer circulation has a single anticyclonic gyre; during a season when w_e weakens, the lower-layer circulation is composed of two counterrotating gyres with an anticyclonic gyre to the north and a cyclonic gyre to the south.

It is somewhat surprising to see that for strong annual forcings (with perturbation Ekman pumping comparable to the mean Ekman pumping), the disturbance is essentially linear. Even under a strong decadal forcing, the linear solution still approximates the nonlinear solution very well in the eastern part of the shadow zone. Nevertheless, the linear perturbation is influenced substantially by the basic-state thermocline structure. The mean thermocline structure results in a divergent group velocity field. This in turn produces a decay effect on Rossby waves downstream. The basic Sverdrup flow creates a ventilated zone where no Rossby waves from the eastern boundary will be allowed to enter and where the advection due to the subducted water is as important as the local response; they tend to cancel each other. In the shadow zone, if the interface is shallower, local responses dominate because the eastern boundary Rossby waves decay rapidly due to the strongly divergent Rossby wave velocity. On the other hand, if the interface is deep, remote Rossby waves dominate because the effective Ekman pumping diminishes toward the interior. For observations, the results here may imply that the relative importance of the local or remote response depends on the depth in the thermocline. In the upper thermocline, local response may dominate, while the opposite may occur for deeper thermocline.

For a strong decadal forcing, the nonlinearity is still weak in the eastern part of the shadow zone but is no longer negligible in the western part of the shadow zone. The maximum nonlinearity occurs about one-quarter wavelength from the eastern boundary. The time-mean thermocline in the shadow zone is always shallower than the steady thermocline under the time-mean Ekman pumping. The difference may be significant, especially in the western part of a shadow zone, where the difference can reach more than O(10) m. This shallower mean thermocline is mainly caused by the nonlinear Rossby wave. The mean lower-layer flow in the shadow zone is no longer at rest. Instead, it is southward.

We should point out some limits of the above theory. First, the eastern boundary interface depths are fixed in this study. This is part of the reason why the nonlinearity is always weak in the eastern part of the shadow zone. In fact, as discussed in Liu (1993c), if we have a disturbance along the eastern boundary, the nonlinearity may become very strong. The nonlinear steepening of the Rossby wave will cause breaking of interface waves.

Second, one should be cautious in applying the conclusion about the relative importance between the local response and the eastern boundary Rossby waves to a continuously stratified model. The two-layer model is a very crude representation in the vertical direction. It is unclear to me how exactly this representation corresponds to a continuously stratified thermocline. More

specifically, we do not know if an interface at a depth resembles the isopycnal with the same depth in a continuously stratified thermocline. Nevertheless, intuitively, it seems that this analogy should hold to some extent. Therefore, the results here are still relevant to more complicated models. Obviously, much work is needed. Particularly, numerical modeling of thermoclines under annual and decadal Ekman pumping is extremely important in verifying the theory here and finding new phenomena.

Acknowledgments. This work was started when the author was working on his Ph.D. thesis in the Joint Program of MIT/Woods Hole Oceanographic Institution. The author is indebted to Dr. J. Pedlosky for his advice and encouragement. Drs. C. Wunsch, G. Flierl, and R. X. Huang have provided helpful suggestions. The careful reading of D. Marshall is greatly appreciated. The comments of two anonymous reviewers are greatly appreciated. One reviewer's suggestion helped the author in finding one error in one equation. This work is partly supported by the Division of Atmospheric Research, NSF, and partly supported by NOAA postdoctoral fellowship in Climate Change.

APPENDIX A

The Approximate Linear Solution at 1 ω^{-2} Order

Here, we derive an approximate expression for the linear wave in (2.15) [or (2.13)] accurate to $1/\omega^2$. Noting the g in (2.2a), along characteristics (therefore f_i, t_i are constants), we can integrate (2.13) by parts to yield

$$h_1 = \frac{1}{\hat{h}_0}\frac{1-\hat{h}_0}{\hat{f}}\left(\frac{-1}{\omega}\right)\int_0^s \hat{f}w_0(\hat{f})\hat{h}_0 d[\cos\omega(t_i+s)]$$

$$= \frac{1}{\hat{h}_0}\frac{1-\hat{h}_0}{\hat{f}}\left(\frac{-1}{\omega}\right)\left\{\hat{f}w_0(\hat{f})\hat{h}_0\cos\omega(t_i+s)\Big|_0^s - \int_0^s \cos\omega(t_i+s)d[\hat{f}w_0(\hat{f})\hat{h}_0]\right\}$$

$$= \frac{1}{\hat{h}_0}\frac{1-\hat{h}_0}{\hat{f}}\left(\frac{-1}{\omega}\right)\left\{\hat{f}w_0(\hat{f})\hat{h}_0\cos\omega(t_i+s) - f_i w_0(f_i)H_s\cos\omega t_i - \frac{1}{\omega}\int_0^s\left[\frac{d\hat{f}}{ds}w_0(\hat{f})\hat{h}_0 + \hat{f}w_{0f}\frac{d\hat{f}}{ds}\hat{h}_0 + \hat{f}w_0(\hat{f})\frac{d\hat{h}_0}{ds}\right]d[\sin\omega(t_i+s)]\right\}.$$

Here, we have used f, $h_0|_{s=0} = f_i$, H_s [see (2.6b,c)]. In the last equality, the first two terms give the $O(1/\omega)$ solution in (2.17) if we use $t_i = t - s$ and (2.8a,c). For the $O(1/\omega^2)$ solution, we first substitute the characteristic equations for the basic state (2.5)

$$\frac{df}{ds} = fw_0, \quad \frac{dh_0}{ds} = -(1-h_0)w_0,$$

into the integral of the last equality. Then, we integrate it by parts again. Using $t_i = t - s$ and (2.8a,c), we obtain

$$h_1 = \frac{(1-h_0)w_0(f)}{\omega}[\cos\omega t - A\cos(\omega t - \Phi)] + O\left(\frac{1}{\omega^3}\right), \quad \text{(A.1a)}$$

where A and Φ are functions of x and f:

$$A = a_0\left[1 + \left(\frac{b_1}{\omega a_0}\right)^2 + \frac{a_1}{\omega a_0}\times\left(\frac{a_1}{\omega a_0} - 2\sin\phi + 2\frac{b_1}{\omega a_0}\cos\phi\right)\right]^{1/2}, \quad \text{(A.1b)}$$

$$\cos(\Phi) = \left(\cos\phi + \frac{b_1}{\omega a_0}\sin\phi\right)\frac{a_0}{A},$$

$$\sin(\Phi) = \left(\sin\phi - \frac{a_1}{\omega a_0} - \frac{b_1}{\omega a_0}\cos\phi\right)\frac{a_0}{A}, \quad \text{(A.1c)}$$

$$a_0 = \frac{H_s F_i w_0(F_i)}{h_0 f w_0(f)}, \quad \phi = \omega(t-t_i) = \omega S(x,f), \quad \text{(A.1d)}$$

$$a_1 = -\left[\left(2 - \frac{1}{h_0}\right)w_0(f) + fw_{0f}(f)\right],$$

$$b_1 = \frac{F_i w_0(F_i)}{f w_0(f)}\left[\left(2-\frac{1}{h_0}\right)w_0(f) + fw_{0f}(f)\right]. \quad \text{(A.1e)}$$

Here F_i, h_0, and S are given in (2.8a), (2.7a), and (2.8c), respectively. Equation (A.1) gives the approximation of (2.15) accurate to $O(1/\omega^2)$. Neglecting the second-order terms (by setting $a_1 = b_1 = 0$), (A.1) becomes (2.17). Equation (A.1) can be expected to be valid for frequencies higher than decadal ($\omega \gg 1$). The second-order correction (due to a_1 and b_1) is very important for shallow interfaces ($H_s \ll 1$). Indeed, when $1/\omega h_0 \sim 1/\omega H_s \geq 1$, the second-order correction becomes comparable to the first order. For the special form of Ekman pumping $w_0(f) = W_0/f$, where W_0 is a negative constant, the second-order solution in (A.1) is the exact linear solution (2.15). On shallow interfaces, the failure of the first-order solution in (2.17) is seen below. If $H_s \to 0$, we have $A \sim a_0 \to 0$. The solution is a purely forced response that fails to satisfy the eastern boundary condition (2.9c).

APPENDIX B

The Mechanism for the Time-Mean Thermocline at High Frequencies in the Shadow Zone

Compared with the decadal forcing case, the annual case exhibits substiantially different time-mean thermocline structure as shown in Fig. 1 and Figs. 7c,d. This is because now the interaction between the barotropic and baroclinic flows becomes the dominant

nonlinear effect. We can analyze the high-frequency case through the weakly nonlinear theory. Inserting (2.3), (2.4) into (2.1b), at $O(a^2)$ order, we have

$$h_{1t} + \mathbf{v}_{B0}\cdot\nabla h_1 + C(h_0)h_{1x} - \mu h_1 = -\nabla\cdot(\mathbf{v}_{B1}h_1) - \frac{1}{2}\left(\frac{dC}{dh_0}h_1^2\right)x, \quad \text{(B.1)}$$

where μ is defined in (2.9b). On the right-hand side, the first term is the barotropic–baroclinic interaction and the second term is due to the nonlinear Rossby wave. For simplicity, in the following analysis, the h_1 solution is approximated to $O(1/\omega) \ll 1$ order in (2.17); $\langle Dh_{bb}\rangle$ and $\langle Dh_{\text{Rossby}}\rangle$ will be used to denote the part of the time mean h_2 forced by the barotropic–baroclinic interaction and nonlinear Rossby wave, respectively. After some tedious algebra, and solving the equation (B.1), at the leading order, we obtain

$$\langle Dh_{bb}\rangle \approx \frac{a^2}{2\omega}\frac{(1-H_s)H_s}{h_0}[w_0(f) - \omega_0(F_i)]\sin\Phi \sim O\left(\frac{a^2}{\omega}\right), \quad \text{(B.2a)}$$

$$\langle Dh\rangle_{\text{Rossby}} \approx \left(\frac{aw_0(f)}{\omega}\right)^2[\gamma_1\cos\Phi + \gamma_2] \sim O\left(\frac{a^2}{\omega^2}\right). \quad \text{(B.2b)}$$

Here F_i, h_0, and Φ are determined in (2.8a), (2.7a), and (2.17b); γ_1 and γ_2 are functions of F_i, h_0, and f. Equation (B.2) shows that the barotropic–baroclinic interaction is much stronger than the nonlinear Rossby wave effect in producing the time-mean component. In addition, since $\langle Dh_{bb}\rangle$ depends on $\sin\Phi$, we should expect to see a wavy structure in $\langle Dh\rangle$ field as shown in Figs. 1b,d,e and Figs. 7c,d. In the figures, the time-mean deviation is very weak (about 1 m) for an annual forcing. Dewar's result seems to overestimate this mean deviation.

It is noteworthy that in (B.2) $\langle Dh\rangle_{bb}$ depends heavily on the meridional gradient of the Ekman pumping. If the Ekman pumping is uniform in space, that is, $w_0(f) = W_0$, it holds that $\langle Dh_{bb}\rangle = 0$ at $O(a^2/\omega)$. [In the *QG* model of Dewar (1989), for $w_0(f) = \text{const}$, it can be shown exactly that the mean disturbance $\langle Dh\rangle = 0$ for any amplitude and frequency of forcing.] Hence, in a subtropical gyre, the time-mean deviation $\langle Dh\rangle$ will be relatively weak in the middle of the gyre.

REFERENCES

Anderson, D. L. T., and P. D. Killworth, 1979: Nonlinear propagation of long Rossby waves. *Deep-Sea Res.*, **26,** 1033–1050.

Cheng, P., and S. G. H. Philander, 1989: Rossby wave packets in baroclinic mean currents. *Deep-Sea Res.*, **36,** 17–37.

Dewar, W., 1987: Planetary shock wave. *J. Phys. Oceanogr.*, **17,** 470–482.

——, 1989: A theory of time-dependent thermocline. *J. Mar. Res.*, **47,** 1–31.

Gill, A. E., and P. P. Niiler, 1973: The theory of the seasonal variability in the ocean. *Deep-Sea Res.*, **20,** 141–177.

Kessler, W., 1989: Observations of long Rossby waves in the northern tropic Pacific. NOAA Tech. Memo., ERL-PMEL-86, 169 pp.

Killworth, P., 1979: On the propagation of stable baroclinic Rossby waves through mean shear flow. *Deep-Sea Res.*, **26A,** 997–1031.

Levitus, S., 1988: Ekman volume fluxes for the world ocean and individual ocean basins. *J. Phys. Oceanogr.*, **18,** 274–279.

Liu, Z., 1991: Time-dependent ventilated thermocline. Ph.D. thesis, Joint Program of MIT/Woods Hole Oceanographic Institution, 208 pp.

——, 1993a: Thermocline forced by varying Ekman pumping. Part I: Spinup and spindown. *J. Phys. Oceanogr.*, **23,** 2502–2522.

——, 1993b: Planetary wave penetration across a gyre boundary. *Dyn. Atmos. Ocean,* in press.

——, 1993c: Interannual planetary wave breaking in the presence of Ekman pumping and mean flows. *J. Fluid Mech.*, submitted.

——, and J. Pedlosky, 1993: Thermocline forced by annual and decadal surface temperature. *J. Phys. Oceanogr.*, **23,** in press.

Luyten, J. R., J. Pedlosky, and H. Stommel, 1983: The ventilated thermocline. *J. Phys. Oceanogr.*, **13,** 292–309.

Pedlosky, J., and W. R. Young, 1983: Ventilation, potential vorticity homogenization and the structure of ocean circulation. *J. Phys. Oceanogr.*, **13,** 2020–2037.

Rhines, P. B., 1986: Vorticity dynamics of the oceanic general circulation. *Annu. Rev. Fluid Mech.*, **18,** 433–447.

——, and W. R. Young, 1982: A theory of the wind-driven circulation I. Mid-ocean gyres. *J. Mar. Res.*, **40**(Suppl.), 559–596.

Roden, G. L., 1976: On the structure and prediction of oceanic fronts. *Nav. Res. Rev.*, **29**(3), 18–35.

Roemmich, D., and C. Wunsch, 1984: Apparent changes in the climatic state of the deep North Atlantic Ocean. *Nature,* **307**(5950), 447–450.

Tabara, B., B. Thomas, and D. Ramsden, 1986: Annual and interannual variability of steric sea level along line P in the northeast Pacific Ocean. *J. Phys. Oceanogr.*, **16,** 1378–1398.

Talley, L. D., and W. B. White, 1987: Estimates of time and space scales at 300 meters in the mid-latitude North Pacific from the TRANSPAC XBT program. *J. Phys. Oceanogr.*, **17,** 2168–2188.

Veronis, G., and H. Stommel, 1956: The action of variable wind stress on a stratified ocean. *J. Mar. Res.*, **15,** 43–75.

White, W. B., 1983: Westward propagation of short-term climatic anomalies in the western North Pacific Ocean from 1964–1974. *J. Mar. Res.*, **41,** 113–125.

——, and J. F. Saur, 1983: Sources of interannual baroclinic waves in the eastern subtropical North Pacific. *J. Phys. Oceanogr.*, **13,** 531–544.

——, and S. Tabara, 1987: Interannual westward-propagating baroclinic long-wave activity on line P in the eastern mid-latitude North Pacific. *J. Phys. Oceanogr.*, **17,** 385–396.